Transition metal nitrogen-rich compounds with all-single-bonded infinite nitrogen chains: Effect of homologous element substitution from tantalum to vanadium

Haizhou Wang,[1] Xing Sun,[1] Zifeng Liu,[2] Wenhui Mi,[2] Chong Zhang,[3] Tao Wang,[1] YuJia Wang,[1] Eva Zurek,[4,*] Hanyu Liu,[2,†] and Miao Zhang[1,‡]

[1]*Department of Physics, School of Sciences, Beihua University, Jilin 132013, China*

[2]*Key Laboratory of Material Simulation Methods and Software of Ministry of Education, College of Physics, Jilin University, Changchun 130012, China*

[3]*School of Chemistry and Chemical Engineering, Nanjing University of Science and Technology, Nanjing 210094, China*

[4]*Department of Chemistry, State University of New York at Buffalo, Buffalo, New York 14260-3000, USA*

(Received 5 December 2025; accepted 21 July 2026; published 12 August 2026)

Nitrogen-rich compounds have emerged as promising candidates for high-energy-density applications owing to their superior energy content and environmental benignity, yet uncovering compounds that integrate high energy density with stability and persistence remains a significant scientific challenge. Building upon the synthesized all-single-bonded framework of *Fdd*2-TaN_5, we perform computational studies where the heaviest group-V element (Ta) was strategically substituted with its lightest congener (V), obtaining VN_5—a novel compound that retains the original orthorhombic *Fdd*2 space group symmetry while exhibiting branched, all-single-bonded nitrogen chains. This compound exhibits a remarkable energy density (E_d) of 5.18 kJ/g, far exceeding that of TaN_5 at 2.02 kJ/g. EXPLO5 calculations reveal that its detonation velocity (V_d) and detonation pressure (P_d) reach 16.33 km/s and 187.4 GPa, all surpassing those of TNT. These exceptional characteristics make VN_5 a highly competitive potential high-energy-density material.

DOI: 10.1103/ff7f-yp2m

I. INTRODUCTION

The rapid development of society drives an ever-increasing demand for energy. As a result, there has been significant interest in high-energy-density materials, as they may be indispensable energy storage materials for modern industry. Polymeric nitrogen and nitrogen-rich compounds have emerged as a prominent research focus owing to their exceptional energy density and environmentally benign characteristics, exhibiting potential applications in propellants, explosives, energy storage, and other fields [1,2]. Nitrogen atoms can form single bonds (160 kJ/mol), double bonds (418 kJ/mol), and triple bonds (954 kJ/mol) with each other. Consequently, the decomposition of polymeric nitrogen or nitrogen-rich compounds releases enormous energy through the transformation of N–N single and double bonds into N≡N triple bonds [3].

Numerous polymeric nitrogen structures have been theoretically predicted; from these, the cubic gauche structure (*cg*-N), layered polymeric nitrogen (LP-N), hexagonal layered polymeric nitrogen (HLP-N), and the black phosphorus structure (BP-N) were successively synthesized under high-pressure conditions at 110 GPa (2000 K) [4], 150 GPa (3000 K) [5], 244 GPa (3300 K) [6], and 140 GPa (4000 K) [7], respectively. Upon depressurization, *cg*-N, LP-N, HLP-N, and BP-N could be quenched to pressures of 42, 52, 66, and 48 GPa, respectively [4–7]. The demanding synthetic requirements and poor ambient-pressure structural stability hinder the broader applicability of these nitrogen allotropes. However, incorporating metal elements (M) with diverse electronic structures is a strategy that could be used to modulate the orbital hybridization and coordination of the nitrogen atoms, thereby creating versatile bonding environments for the synthesis of novel polymeric structures with enhanced structural stability.

A wide range of metal nitrides have been reported in theoretical studies [8–24], and several of these nitrogen-rich compounds have been successfully synthesized experimentally [25–32]. For instance, in 2023, two nitrogen-rich compounds K_2N_{16} and KN_5 were synthesized [25]. K_2N_{16} features a layered structure composed of N_{18} rings, remaining stable above 50 GPa with a high energy density of 7.54 kJ/g, while KN_5 demonstrates stability beyond 21 GPa. In 2024, two additional nitrogen-rich compounds LaN_8 and LaN_{16} were successfully synthesized [26]. LaN_8 adopts a layered N_{18}-ring structure stable above 13 GPa, while LaN_{16} features a ribbonlike N_{18}-ring architecture stable beyond 2.2 GPa. Notably, their stabilization pressures are significantly lower than those of polymeric nitrogen. However, the heavy lanthanum constituent results in relatively low energy densities of 2.3 and 3.4 kJ/g, respectively, which are inferior to

*Contact author: ezurek@buffalo.edu
†Contact author: hanyuliu@jlu.edu.cn
‡Contact author: zhangmiaolmc@126.com

conventional explosives like TNT (4.3 kJ/g). In 2021, Bykov *et al.* [30] successfully synthesized TaN_4 and TaN_5 under high-pressure and high-temperature conditions. Significantly, TaN_5 represents the first experimentally realized branched infinite all-single-bonded nitrogen chain structure, demonstrating stability above 35 GPa. This configuration holds particular promise for energy storage applications, as nitrogen-nitrogen single bonds exhibit superior energy storage characteristics. However, due to the high atomic weight of tantalum, the compound achieves an energy density of 2.02 kJ/g. In 2025, Chen *et al.* [33] successfully synthesized NbN_4 and NbN_5 through high-pressure and high-temperature experiments. Notably, the obtained NbN_5 does not feature an all-single-bonded structure.

As is well established in chemistry, elements within the same group exhibit similar physical and chemical properties. For instance, in alkali metals, a 1:5 metal-to-nitrogen ratio consistently favors the formation of N_5^- [8–12]; all-single-bonded nitrogen chain structures coordinated with lighter metal elements may represent a promising strategy for developing high-energy-density materials. Therefore, in this work, we employed an elemental substitution approach based on the TaN_5 structures, replacing the group 5 element Ta with its lighter congener V [34], yielding VN_5 compounds featuring all-single-bonded nitrogen chains. Theoretical simulations revealed that VN_5 is thermally stable to at least 300 K under ambient pressure, and it exhibits an energy density of 5.18 kJ/g at 0 K and 1 atm. Furthermore, our first-principles calculations systematically characterized the key performance parameters of VN_5 at 1 atm, including detonation velocity (V_d), detonation pressure (P_d), and Vickers hardness (H_v).

II. METHODS

In this work, a VN_5 phase with *Fdd*2 space group was created by substituting V for Ta, using a synthesized TaN_5 compound as a prototype. First-principles calculations were performed using density functional theory (DFT) within the Perdew-Burke-Ernzerhof for solids (PBEsol) parametrization of the generalized gradient approximation as implemented in the Vienna *ab initio* simulation package VASP code [35–37]. We used projector augmented wave potentials in which the valence electrons for the V, Nb, Ta, and N atoms were $3p^6\,3d^4\,4s^1$, $4p^6 4d^4 5s^1$, $5p^6 5d^3 6s^2$, and $2s^2 2p^3$. An energy cutoff of 800 eV and dense Gamma k-mesh spacing of $0.03 \times 2\pi$ Å^{-1} were used to ensure that the total energies were converged to within around 1 meV/atom in the structural optimizations. To validate the convergence of the computational parameters chosen, tests were performed, and these are described in the "Verification of computational parameters" section of the Supplemental Material [46]. The phonon dispersion spectra were calculated using the finite displacement method as implemented in the PHONOPY code [38]. The anharmonic phonon dispersion curves were calculated using the DynaPhoPy software package [39]. The chemical bonding interactions were characterized using the crystal orbital Hamiltonian population (COHP) and crystal orbital bond index (COBI) analysis implemented in the LOBSTER code [40,41]. To comprehensively evaluate the detonation performance of VN_5, the detonation velocity and detonation pressure (V_d and P_d) were determined using three independent computational methods: the D-Hug methodology [42], the thermochemical code EXPLO5 [43,44], and the widely used Kamlet-Jacobs empirical formula [45]. The Kamlet-Jacobs empirical equation is given as

$$V_d = 1.01(NM^{0.5}{E_d}^{0.5})^{0.5}(1 + 1.30\rho), \quad (1)$$

$$P_d = 15.88\rho^2 NM^{0.5}{E_d}^{0.5}. \quad (2)$$

In this formula, ρ is the mass density, and N and M represent the moles of nitrogen gas per gram of the crystal and the molar mass (28 g/mol) of dinitrogen gas, respectively.

Additional computational convergence tests and validation data can be found in the Supplemental Material [46].

III. RESULTS

Our calculations began with the *Fdd*2-TaN_5 structure synthesized by Bykov *et al.* and the isostructural NbN_5 synthesized by Chen *et al.*, where the Ta and Nb atoms were replaced by the lightest group 5 element, V, and subject to local relaxation by DFT calculations. Full structural optimizations from 0 to 150 GPa confirmed that both configurations maintain branched, all-single-bonded infinite nitrogen chains while preserving the original orthorhombic *Fdd*2 (No. 43) symmetry space group. Experimental studies have demonstrated that such nitrogen-rich compounds can be synthesized from their metallic elements and nitrogen gas. Following the precedent of LaN_{16} [26], our enthalpy difference calculations reveal that *Fdd*2-VN_5 can be synthesized from V/N_2 mixtures at pressures of 16.0 GPa, as shown in Fig. 1(a). To determine whether this phase is thermodynamically stable with respect to other VN_x phases, we further calculated their formation enthalpies (ΔH_f) and plotted the so-called convex hull [Fig. 1(b)]. Notably, both VN [47,48] and VN_2 [49] have been experimentally synthesized. The results demonstrate that VN_5 becomes thermodynamically stable at 120 GPa, while at 50 and 100 GPa, its distance to the convex hull measures 136 and 33 meV/atom, respectively. Simultaneously, calculations reveal that VN_5 exhibits no imaginary frequencies in its phonon dispersion curve at 110 GPa (Fig. S1 of the Supplemental Material [46]). Molecular dynamics simulations confirm structural stability under conditions of 120 GPa and 2000 K (Fig. S2 of the Supplemental Material [46]); therefore, we conclude that VN_5 could likely be synthesized at pressures above ~120 GPa [50].

At 1 atm, VN_5, NbN_5, and TaN_5 can decompose into the thermodynamically stable phases. NbN_5 decomposes into NbN and N_2, and TaN_5 decomposes into Ta_3N_5 and N_2 [30,33]. Considering only the decomposition pathways to the lowest point on the convex hull, VN_5 decomposes into VN [47,48] and N_2. Therefore, the decomposition pathways can be expressed as $VN_5 \rightarrow VN + 2N_2$, $NbN_5 \rightarrow NbN + 2N_2$, $3TaN_5 \rightarrow Ta_3N_5 + 5N_2$. In Fig. 1(c), we plot the enthalpy difference between *Fdd*2-MX_5 and their potential decomposition products. All three compounds are predicted to decompose at atmospheric pressures, with VN_5 having the largest enthalpy difference and thus releasing the highest amount of energy. At pressures below 49.8, 37.0, and 40.2 GPa, respectively, VN_5, NbN_5, and TaN_5 are thermodynamically preferred

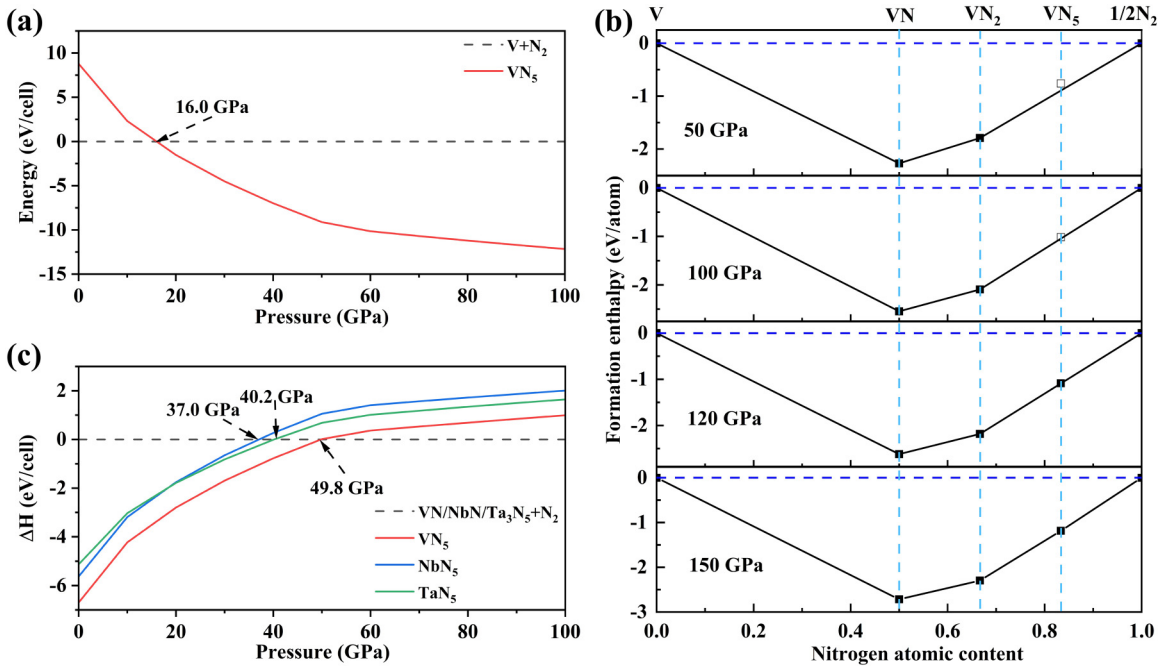

FIG. 1. (a) The enthalpy-pressure relationships of *Fdd*2-VN_5 relative to the V and N_2 mixture. (b) The formation enthalpies of VN_x phases with respect to vanadium and ½ N_2 at different pressures. (c) The enthalpy-pressure relationships of VN_5, NbN_5, and TaN_5 relative to the decomposition products VN/NbN/Ta_3N_5 and N_2. [The *Im*-3*m* phase of elemental V and the α-N_2 (0 GPa), ε-N_2 (1–56 GPa), and *cg*-N_2 (56–150 GPa) phases were used in the calculations.]

toward decomposition into VN, NbN, Ta_3N_5, and N_2. In the following section, we discuss the structures and properties of VN_5.

VN_5 maintains structural stability within a pressure range of 0–150 GPa. At 1 atm, the lattice parameters are determined to be $a = 14.1979$ Å, $b = 12.6081$ Å, $c = 3.7126$ Å, and $\alpha = \beta = \gamma = 90.0^\circ$. The crystal structure of VN_5 at ambient pressure reveals that N4 and N1 alternate to form a chairlike nitrogen chain extending infinitely along the *c* axis. The side chain consists of N3, N2, and N5 atoms, where N5 is connected to N4 and terminates at the N3 atom [Figs. 2(a) and 2(b)]. At 1 atm, the N–N bond lengths in VN_5 range from 1.397 to 1.515 Å, consistent with typical N–N single bonds, while the bond angles vary between 102.0° and 112.7° [Fig. 2(c)]. The longest N5–N4 bond is further analyzed by the electron localization function (ELF), where an isosurface value of 0.8 indicates covalent bond formation between N4 and N5 (Fig. S3 of the Supplemental Material [46]). Additionally, each vanadium atom is coordinated by ten surrounding nitrogen atoms [Fig. 2(d)], forming ionic bonds with characteristic interatomic distances ranging from 2.071 to 2.483 Å.

The phonon dispersion curves of VN_5 at 0 K and 1 atm exhibit no imaginary frequencies, demonstrating its dynamic stability, as clearly shown in Fig. 3(a). To gain deeper insight into the bonding and stabilization mechanisms of VN_5, we systematically investigated its electronic properties at 0 K and 1 atm, including band structure, projected density of states (PDOS), Bader charge analysis, and COHP calculations. Figure 3(b) displays the projected electronic band structure of VN_5 along with the corresponding PDOS, where the total density of states is represented by the black curve, while the red, blue, and yellow curves correspond to the partial density of states originating from N 2*s*, N 2*p*, and V 3*d* states, respectively. The results clearly demonstrate that VN_5 exhibits semiconducting characteristics with an indirect band gap of 0.21 eV (within the PBEsol functional, which is known to underestimate band gaps), between the valence band maximum at (0.16, 0, 0.16) and the conduction band minimum at the Z special point. The PDOS analysis reveals overlap between the N 2*p* and V 3*d* states and a large amount of V 3*d* character below the Fermi level, indicating strong interactions and pronounced hybridization between these orbitals. Additionally, we calculated the charge transfer between V and N atoms using a Bader analysis. The total charge transferred from one V atom to all of the N atoms is 1.84*e*, suggesting a +2 oxidation state on the metal atom, with the amount donated to each nitrogen listed in Fig. 3(c). However, a Bader analysis often underestimates the formal oxidation state [51]. Assuming full electron transfer, that is, a +5 oxidation state on the V metal, we drew the VN_5 Lewis structure shown in Fig. 3(d). Among the nitrogen atoms, the terminal N3 atom possesses three lone electron pairs, while N1, N2, and N5, which are each singly bonded to two other nitrogen atoms, each possess two lone electron pairs, and N4, with three single N–N bonds, possesses one lone pair.

The above analysis assumes a fully ionic picture; however, as already suggested by the Bader charges, full charge transfer of the electrons from the metal to the nitrogens does not occur. In fact, visualization of the ELF, in Fig. 3(e), suggests the potential for N–V covalent bond formation, rendering each nitrogen atom quasitetrahedrally coordinated (Table SI of the

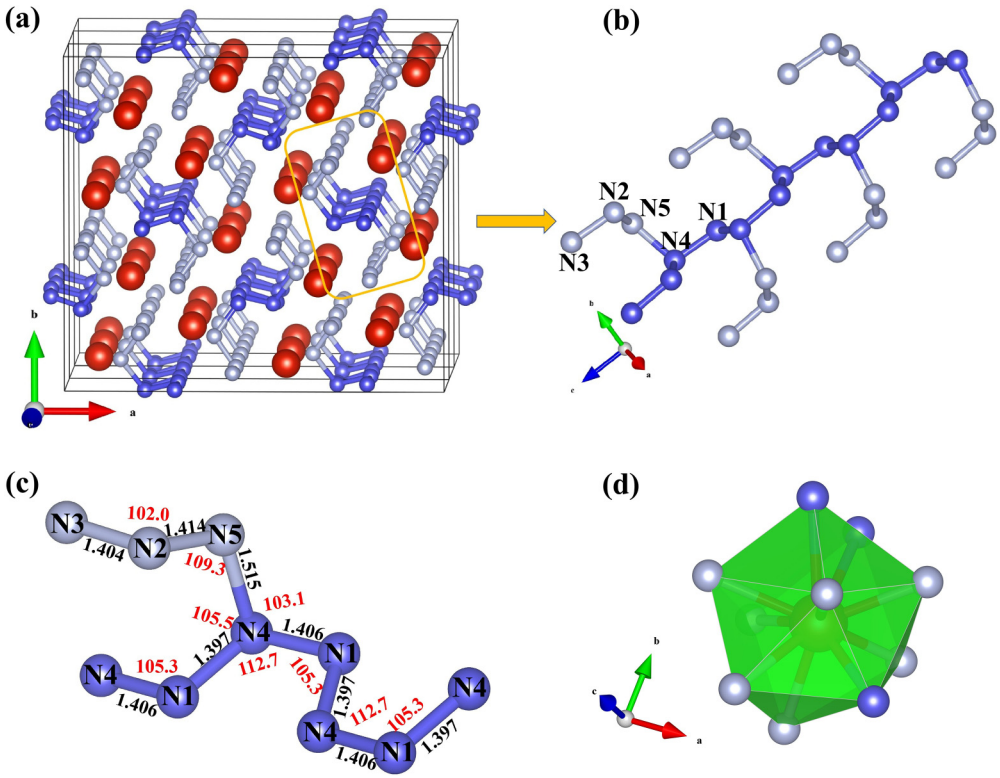

FIG. 2. The structure of VN_5 optimized at 0 K and 1 atm. The red spheres represent the positions of V atoms, while the gray and blue spheres denote the nitrogen atoms in the branched and polymeric chains, respectively. (a) Stereoscopic view. (b) Polymeric nitrogen units in VN_5. (c) The black and red numbers denote the bond length (unit: Å) and N–N–N angles (unit: °), respectively. (d) Coordination environment of V atoms.

Supplemental Material [46]). The N3 atom is connected to three V atoms and one N atom, the N4 atom is connected to one V atom and three N atoms, and N1, N2, and N5 are each connected to two V atoms and two N atoms. Therefore, all nitrogen atoms exhibit sp^3 hybridization, in line with each N atom being fully single bonded.

COHP and COBI are powerful tools for quantitative characterization of the strength of chemical bonds in solids. The projected COHP (pCOHP) and the integral of the COHP to the Fermi level (ICOHP) can be used to show which energy ranges, relative to the Fermi level, are involved in forming (covalent) bonding and antibonding interactions, and the strength of those interactions, respectively. In addition to providing results for each pair of nitrogen atoms, an average (N–N) is given, as is the average V–N interaction. Bonding and antibonding contributions are represented by positive and negative values of −pCOHP, respectively. Integrated crystal orbital bond index (ICOBI) can intuitively quantify the bond order of covalent bonds in solid-state materials. As shown in Fig. 4(a), the V–N bonding states are full and the antibonding ones are empty, while some of the N–N antibonding states are populated. Furthermore, the ICOHP values averaged over the N–N bonds are computed to be −11.18 eV, whereas the V–N bond strength averaged over all interactions is −2.04 eV (Table I). The average ICOBI of the N–N bond is approximately 0.97, while that of the V–N bond is approximately 0.40 (Table I). Based on this, we can conclude that the N–N bond exhibits strong covalent single-bond character, whereas the V–N bond is primarily dominated by ionic bonding, accompanied by weak covalent interactions. This picture is further corroborated with the previously presented PDOS and ELF analysis.

As shown in Table I, ICOHP analysis shows that at 35 GPa, the average ICOHP value of N–N bonds in TaN_5 is −10.82 eV, while that of Ta–N bonds is −3.25 eV. These results indicate that the covalent interactions within the nitrogen chain of VN_5 at 1 atm are stronger than those in TaN_5 at 35 GPa. As shown in Fig. S5 of the Supplemental Material [46], all N–N bond lengths elongate upon decompression, with the N5–N4 bond increasing more than the other N–N bonds, indicating that this bond is more susceptible to pressure-induced breaking. However, as the pressure decreases and the magnitude of the −ICOHP gradually decreases, the ICOBI value for this bond remains consistently above 0.84, indicating that the degree of interorbital electron sharing still exhibits the characteristics typical of a single N–N bond. At 1 atm, the ICOHP value for N5–N4 in VN_5 is −8.44 eV, significantly less negative than the average value of −11.18 eV, indicating that the N5–N4 bond is less strong than the other nitrogen-nitrogen bonds, in line with its longer distance (1.515 Å versus an average of 1.427 Å). We further calculated the ICOHP value of the N5–N4 bond for TaN_5 at 35 GPa to be −7.73 eV, showing that it is weaker than the N5–N4 bond in VN_5. The enhanced N-N bond strength could be correlated with the ionic radii of the metal cations. Compared with Ta^{5+} (0.64 Å), the smaller ionic radius of V^{5+} (0.54 Å) more effectively draws electron density toward the N–N bonding region. This effect shortens the N–N bonds and reinforces covalent interactions along the

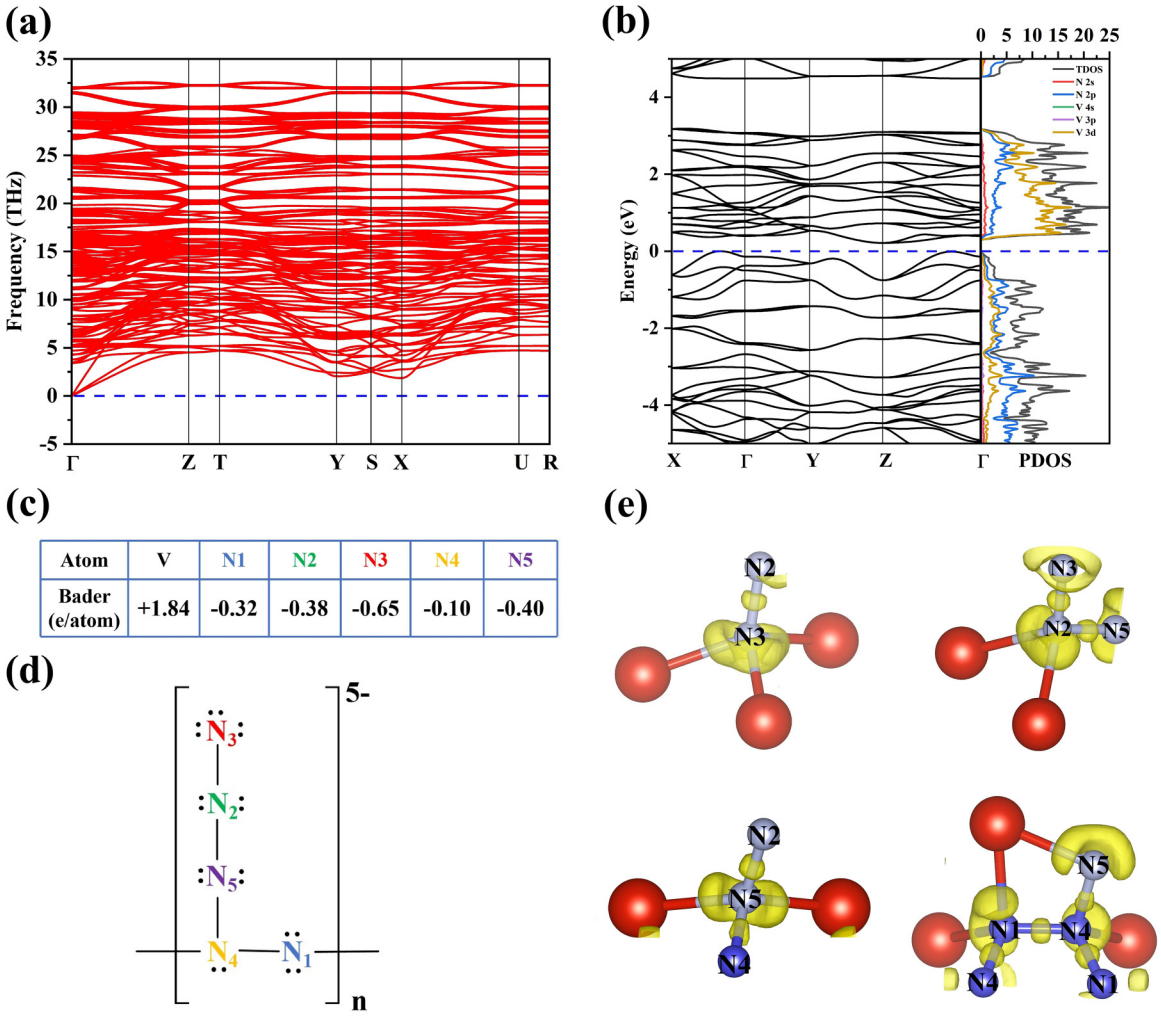

FIG. 3. (a) Phonon dispersion curves of VN_5, calculated at 1 atm and 0 K. (b) Band structure and PDOS plot of VN_5, calculated at 1 atm and 0 K. (c) Bader charge analysis of VN_5, calculated at 1 atm and 0 K. (d) Lewis structure diagram of the nitrogen chain in VN_5 at 1 atm and 0 K. (e) Electron localization function (ELF) contour plot (isovalue = 0.8) of VN_5, calculated at 1 atm and 0 K.

chain, in line with the finding that VN_5 is a local minimum at 1 atm, but TaN_5 is not.

To investigate the stability of the VN_5 structure at 300 K, we conducted *ab initio* molecular dynamics (AIMD) simulations at 1 atm for temperatures of 300 K, as well as at 30 GPa and 300 K. As shown in Fig. 5(a), during the first 8 ps of the AIMD simulation at 1 atm and 300 K, the total energy decreased slightly by approximately 3 eV (15 meV/atom) and remained stable thereafter, indicating thermal equilibration. Therefore, we calculated the anharmonic phonon dispersion curves for the 8–20 ps time interval; no imaginary frequencies were observed, as shown in Fig. 5(b), demonstrating the dynamic stability of VN_5 at 300 K. We then extracted the instantaneous structure at 8 ps [Fig. S6 of the Supplemental Material [46]], and further evaluated structural evolution via root-mean-square deviation (RMSD) [Fig. S7(a) of the Supplemental Material [46]] and mean squared displacement (MSD) [Fig. S8(a) of the Supplemental Material [46]] within the 8–20 ps time interval. The RMSD curve remained at a consistently low level, with an average value of 0.255 Å

TABLE I. The −ICOHP values and ICOBI values for VN_5 and TaN_5 at 0 K and the listed pressure.

			Bond						
	System	Pressure (GPa)	V–N/Ta-N	N–N	N3–N2	N2–N5	N5–N4	N4–N1	N1–N4
−ICOHP (eV/bond)	VN_5	0	2.04	11.18	12.10	11.57	8.44	11.80	11.98
	TaN_5	35	3.25	10.83	10.75	12.12	7.73	11.27	12.27
ICOBI	VN_5	0	0.40	0.97	1.04	0.99	0.84	0.99	0.99
	TaN_5	35	0.45	0.95	1.03	0.99	0.79	0.97	0.96

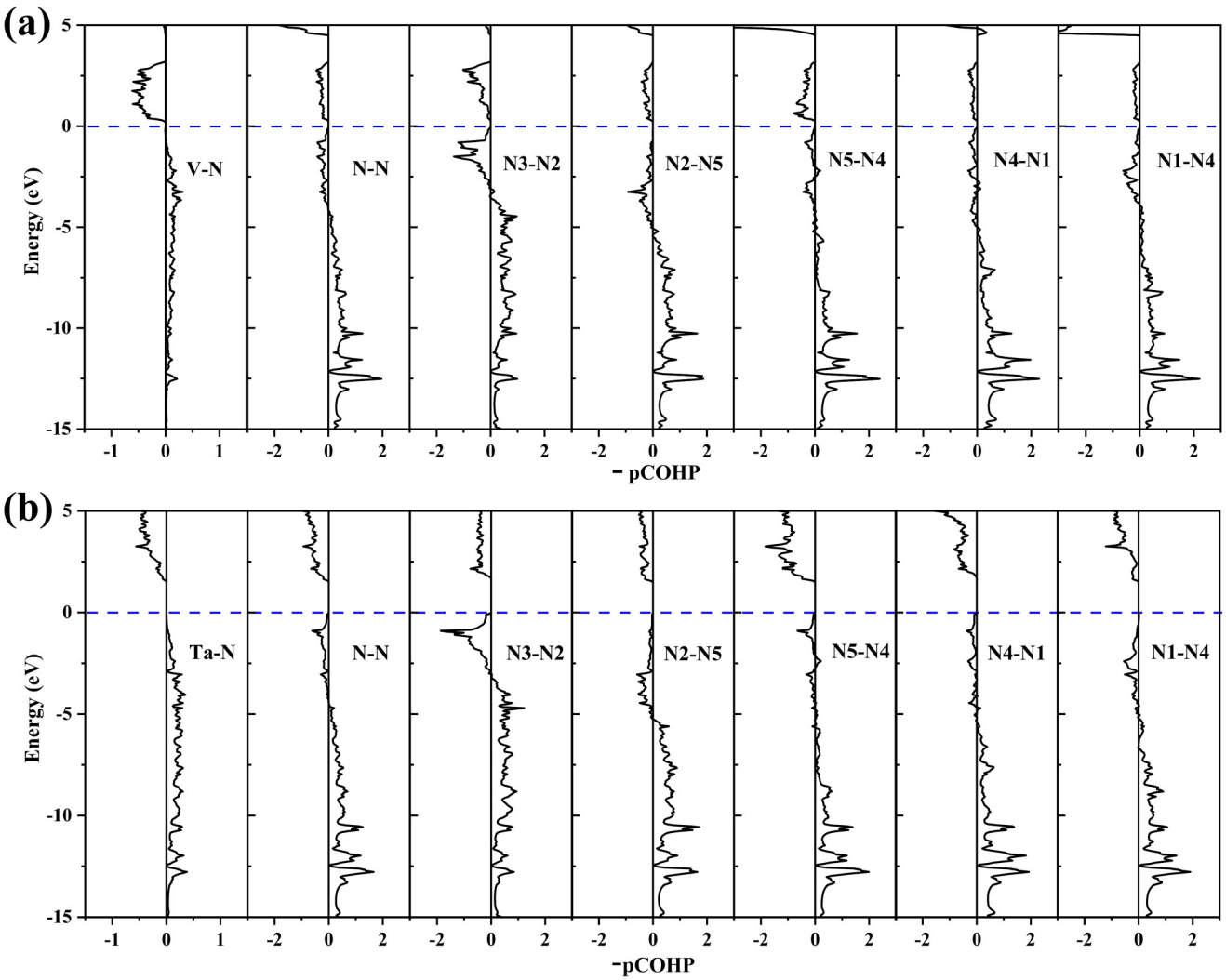

FIG. 4. (a) Plots of the COHP for select N_x–N_y and average N–N and V–N bonds in VN_5, calculated at 0 K and 1 atm. (b) Plots of the COHP for select N_x–N_y and average N–N and Ta–N bonds in TaN_5, calculated at 35 GPa and 0 K. The negative region on the left represents antibonding states, while the positive region on the right corresponds to bonding states. The dashed line indicates the Fermi level.

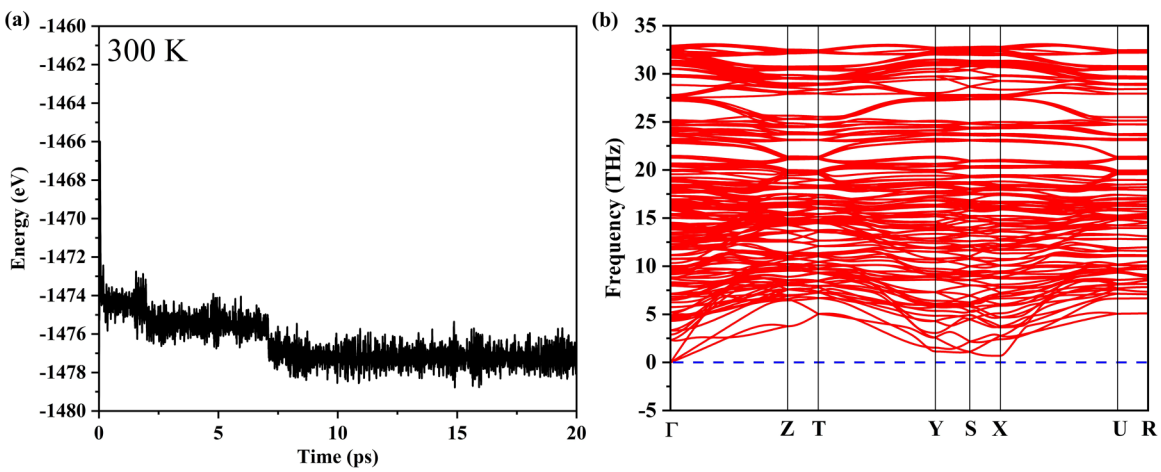

FIG. 5. (a) Total energy vs time in AIMD simulations of VN_5 at 1 atm and 300 K. (b) Anharmonic phonon dispersion curves of VN_5 at 1 atm and 300 K.

TABLE II. The elastic constants C_{ij}; and bulk modulus (B), shear modulus (G), and Vickers hardness values (in units of GPa) of VN_5, calculated at 0 K and 1 atm.

	C_{11}	C_{22}	C_{33}	C_{44}	C_{55}	C_{66}	C_{12}	C_{13}	C_{23}
VN_5	622.8	537.4	971.4	159.3	255.2	251.3	128.1	100.2	37.3

B	G	G/B	H_v^{Chen}	H_v^{Tian}
289.3	246.4	0.85	38.6	37.8

(Table SIII of the Supplemental Material [46]), confirming that the structure experienced only minor thermal vibrations without significant distortion. Although some N5–N4 bonds elongated to approximately 2 Å, the MSD oscillated around a plateau, indicating that the atoms did not undergo significant drift and that the overall structure remained stable. Therefore, these three methods collectively confirm the structural stability of VN_5 under conditions of 1 atm and 300 K.

In contrast, under high-pressure conditions of 30 GPa and 300 K (Fig. S9 of the Supplemental Material [46]), the total energy of VN_5 fluctuated stably around its average value, and the crystal structure remained intact throughout the 20 ps simulation, with no weakening of chemical bonds. Furthermore, the RMSD remained extremely low and stable throughout the equilibrium phase, with an average value of approximately 0.202 Å (Table SIII of the Supplemental Material [46]), confirming that the VN_5 structure undergoes only slight thermal vibrations under high pressure, with no significant structural distortion. Meanwhile, the MSD also exhibits stable oscillations between 1 and 20 ps, indicating that atomic drift is negligible and atomic migration is suppressed. These results suggest that the structural stability of VN_5 is further enhanced under a compression of 30 GPa.

We further conducted simulations to calculate the elastic constants of VN_5 to study its mechanical properties. Additionally, we used different empirical models to calculate the bulk modulus, shear modulus, and hardness values. As shown in Table II, the results indicate that this phase satisfies the orthorhombic crystal system's mechanical stability criteria, confirming the mechanical stability of VN_5 at 0 K and 1 atm. Furthermore, VN_5 exhibits a bulk modulus $B = 289.3$ GPa and shear modulus $G = 246.4$ GPa, demonstrating exceptional resistance to compressive and shear deformation. We further estimated the Vickers hardness (H_v) using Chen *et al's* [52] and Tian *et al*'s [53] hardness models based on shear modulus-hardness correlation; VN_5 is a hard material at ambient pressure with a Vickers hardness value of ∼38 GPa. This high hardness is attributed to the synergistic resistance to external deformation provided by the strong covalent N–N bonds (ICOHP = −11.18 eV) and the rigid ionic-covalent V–N coordination framework.

The decomposition of nitrogen-rich compounds releases substantial energy. At 1 atm, the complete decomposition products of VN_5 are VN [47,48] and N_2 (Fig. S10 of the Supplemental Material [46]). Therefore, the decomposition pathways can be expressed as $VN_5 \rightarrow VN + 2N_2$. Based on the decomposition pathway, we calculated the gravimetric energy density and detonation heat of VN_5 at 0 K and 1 atm, as summarized in Table III. The results demonstrate that VN_5 exhibits a gravimetric energy density of 5.18 kJ/g, more than double that of TaN_5, surpassing that of TNT and approaching that of HMX. Compared to polymeric nitrogen, its energy density is only half that of *o*-N16 and *cg*-N [56], as shown in Table SIV of the Supplemental Material [46]. This value represents the total chemical energy potential. However, as the vanadium metal primarily serves to stabilize the structure and does not participate in energy release, the actual detonation heat per unit mass is relatively low. Specifically, the actual detonation heat release predicted by the thermochemical code EXPLO5 is −2.44 kJ/g, approximately half that of TNT. The actual detonation heat release predicted by the D-Hug methodology is −4.18 kJ/g, comparable to the detonation heat of TNT. Detonation velocity and detonation pressure serve as key parameters for evaluating high-energy-density materials. We employed three distinct computational methods to predict the detonation velocity of VN_5 and calculated the detonation pressure using the EXPLO5 and Kamlet-Jacobs empirical formulas, as shown in Table IV. Our predicted detonation velocities for VN_5 are 11.30, 16.33, and 18.48 km/s, approximately twice that of TNT. The corresponding detonation pressures reach 187.3 and 229.8 GPa, approximately ten times that of TNT. These exceptional theoretically predicted explosive properties highlight the significant potential of VN_5 and warrant its serious consideration for future experimental exploration as a possible high-energy-density material.

TABLE III. Computational properties of VN_5 and their comparison with NbN_5, TaN_5, TNT, and HMX, including mass density (ρ), energy density (E_d), and detonation heat. VN_5 data originate from DFT calculations conducted in this study at 0 K and 1 atm. The pressure conditions for NbN_5, TaN_5, TNT, and HMX are 1 atm. The D-Hug methodology results are denoted as D-Hug, while EXPLO5 results are denoted as EXPLO5.

Compounds	ρ (g/cm^3)	E_d (kJ/g)	Detonation heat (kJ/g) D-Hug	EXPLO5
VN_5	4.84	5.18	−4.18	−2.44
NbN_5	–	2.76[a]	–	–
TaN_5	–	2.02[b]	–	–
TNT	1.64[c]	4.30[d]	−3.90[e]	−4.39[f]
HMX	1.90[c]	5.70[d]	−5.92[e]	−6.03[g]

[a]Reference [33].
[b]Reference [30].
[c]Reference [54].
[d]Reference [55].
[e]Reference [42].
[f]Reference [44].
[g]Reference [43].

IV. CONCLUSIONS

In conclusion, density functional theory calculations demonstrate that strategic homologous replacement of Ta by the lighter congener V successfully transforms TaN_5 into isostructural VN_5 while preserving the orthorhombic *Fdd*2 framework and its unique all-single-bonded, branched nitrogen chains. Comprehensive first-principles calculations show that the mass reduction afforded by vanadium elevates the

TABLE IV. Computational properties of VN_5 and comparison with TNT and HMX, including detonation velocity (V_d) and detonation pressure (P_d). The density of VN_5 was calculated at 0 K and 1 atm, while the pressure conditions for TNT and HMX are 1 atm. Calculation methods included the D-Hug method, the EXPLO5 model, and the Kamlet-Jacobs empirical formula. Tables are labeled D-Hug, EXPLO5, and K-J, respectively.

Compounds	ρ (g/cm^3)	V_d (km/s) D-Hug	V_d (km/s) EXPLO5	V_d (km/s) K-J	P_d (GPa) D-Hug	P_d (GPa) EXPLO5	P_d (GPa) K-J
VN_5	4.84	11.30	16.33	18.48	–	187.4	229.8
TNT	1.6	6.7[a]	–	–	19.0[a]	–	–
TNT	1.64	–	6.75[b]	–	–	18.1[b]	–
TNT	1.64		6.90[c]			19.0[e]	
HMX	1.91	8.6[a]	–	–	31.2[a]	–	–
HMX	1.89	–	9.21[d]	–	–	37.8[d]	–
HMX	1.90		9.10[c]			39.3[e]	

[a]Reference [42].
[b]Reference [44].
[c]Reference [57].
[d]Reference [43].
[e]Reference [54].

gravimetric energy density to 5.18 kJ/g, more than doubling that computed for TaN_5 and surpassing TNT. Simultaneously, VN_5 delivers exceptional detonation parameters—16.33 km/s and 187.4 GPa—owing to its high density (4.84 g/cm^3) and the large heat release from N–N single-bond conversion to N_2. Phonon spectra and elastic constants confirm dynamic and mechanical stability from 0 to 150 GPa, with a Vickers hardness of ∼38 GPa at 1 atm. Charge and bonding analyses are indicative of covalent N–N bonding reinforced by mixed covalent/ionic V–N interactions that anchor the nitrogen chains at ambient pressure and low temperatures, with partial nitrogen chain dissociation by 300 K. The predicted synthesis threshold (∼120 GPa) is lower than the threshold for most polymeric nitrogen-containing phases (110–244 GPa); these attributes suggest that VN_5 has the potential to be a next-generation, environmentally benign high-energy-density material that simultaneously delivers extreme mechanical strength and exceptional explosive performance.

ACKNOWLEDGMENTS

This work was supported by the Jilin Provincial Science and Technology Development Joint Fund Project (Grant No. YDZJ202601ZYTS032). E.Z. acknowledges the National Science Foundation, Grant No. DMR-2119065.

DATA AVAILABILITY

There are no publicly available research data or software supporting this manuscript. Requests for further information or data should be sent to the authors.

[1] R. P. Singh, H. Gao, D. T. Meshri, and J. M. Shreeve, Nitrogen-rich heterocycles, in *High Energy Density Materials. Structure and Bonding* (Springer, Berlin, Heidelberg, 2007), Vol. 125.

[2] A. Hammerl, T. M. Klapötke, H. Nöth, M. Warchhold, and G. Holl, Synthesis, structure, molecular orbital and valence bond calculations for tetrazole azide, CHN_7, Propellants, Explos. Pyrotech. **28**, 165 (2003).

[3] H. K. Mao, C. Ji, B. Li, G. Liu, and E. Gregoryanz, Extreme energetic materials at ultrahigh pressures, Engineering **6**, 976 (2020).

[4] M. I. Eremets, A. G. Gavriliuk, I. A. Trojan, D. A. Dzivenko, and R. Boehler, Single-bonded cubic form of nitrogen, Nat. Mater. **3**, 558 (2004).

[5] D. Tomasino, M. Kim, J. Smith, and C.-S. Yoo, Pressure-induced symmetry-lowering transition in dense nitrogen to layered polymeric nitrogen (LP-N) with colossal Raman intensity, Phys. Rev. Lett. **113**, 205502 (2014).

[6] D. Laniel, G. Geneste, G. Weck, M. Mezouar, and P. Loubeyre, Hexagonal layered polymeric nitrogen phase synthesized near 250 GPa, Phys. Rev. Lett. **122**, 066001 (2019).

[7] C. Ji *et al.*, Nitrogen in black phosphorus structure, Sci. Adv. **6**, eaba9206 (2020).

[8] F. Peng, Y. Yao, H. Liu, and Y. Ma, Crystalline LiN_5 predicted from first-principles as a possible high-energy material, J. Phys. Chem. Lett. **6**, 2363 (2015).

[9] B. A. Steele and I. I. Oleynik, Novel potassium polynitrides at high pressures, J. Phys. Chem. A **121**, 8955 (2017).

[10] B. A. Steele and I. I. Oleynik, Sodium pentazolate: A nitrogen rich high energy density material, Chem. Phys. Lett. **643**, 21 (2016).

[11] A. S. Williams, B. A. Steele, and I. I. Oleynik, Novel rubidium poly-nitrogen materials at high pressure, J. Chem. Phys. **147**, 234701 (2017).

[12] F. Peng, Y. Han, H. Liu, and Y. Yao, Exotic stable cesium polynitrides at high pressure, Sci. Rep. **5**, 16902 (2015).

[13] Y. Zhang, L. Wu, B. Wan, Y. Lin, Q. Hu, Y. Zhao, R. Gao, Z. Li, J. Zhang, and H. Gou, Diverse ruthenium nitrides stabilized under pressure: A theoretical prediction, Sci. Rep. **6**, 33506 (2016).

[14] S. Zhang, Z. Zhao, L. Liu, and G. Yang, Pressure-induced stable BeN_4 as a high-energy density material, J. Power Sources **365**, 155 (2017).

[15] S. Wei, D. Li, Z. Liu, X. Li, F. Tian, D. Duan, B. Liu, and T. Cui, Alkaline-earth metal (Mg) polynitrides at high pressure as possible high-energy materials, Phys. Chem. Chem. Phys. **19**, 9246 (2017).

[16] S. Zhu, F. Peng, H. Liu, A. Majumdar, T. Gao, and Y. Yao, Stable calcium nitrides at ambient and high pressures, Inorg. Chem. **55**, 7550 (2016).

[17] S. Wei, L. Lian, Y. Liu, D. Li, Z. Liu, and T. Cui, Pressure-stabilized polymerization of nitrogen in alkaline-earth-metal strontium nitrides, Phys. Chem. Chem. Phys. **22**, 5242 (2020).

[18] S. Niu, Z. Li, H. Li, X. Shi, Z. Yao, and B. Liu, New cadmium–nitrogen compounds at high pressures, Inorg. Chem. **60**, 6772 (2021).

[19] S. Liu, R. Liu, H. Li, Z. Yao, X. Shi, P. Wang, and B. Liu, Cobalt–nitrogen compounds at high pressure, Inorg. Chem. **60**, 14022 (2021).

[20] L. Liu, D. Wang, S. Zhang, and H. Zhang, Pressure-stabilized GdN_6 with an armchair–antiarmchair structure as a high energy density material, J. Mater. Chem. A Mater. **9**, 16751 (2021).

[21] L. Wu, R. Tian, B. Wan, H. Liu, N. Gong, P. Chen, T. Shen, Y. Yao, H. Gou, and F. Gao, Prediction of stable iron nitrides at ambient and high pressures with progressive formation of new polynitrogen species, Chem. Mater. **30**, 8476 (2018).

[22] S. Niu, D. Xu, H. Li, Z. Yao, S. Liu, C. Zhai, K. Hu, X. Shi, P. Wang, and B. Liu, Pressure-stabilized polymerization of nitrogen in manganese nitrides at ambient and high pressures, Phys. Chem. Chem. Phys. **24**, 5738 (2022).

[23] Z. Liu, D. Li, S. Wei, Y. Liu, F. Tian, D. Duan, and T. Cui, Nitrogen-rich GaN_5 and GaN_6 as high energy density materials with modest synthesis condition, Phys. Lett. A **383**, 125859 (2019).

[24] P. Patel, S. Patel, M. H. Dalsaniya, D. Kurzydłowski, K. J. Kurzydłowski, and P. K. Jha, Exploration of Si–N compounds as high energy density materials, Phys. Chem. Chem. Phys. **26**, 25089 (2024).

[25] M. Sui *et al.*, High-pressure synthesis of fully sp^2-hybridized polymeric nitrogen layer in potassium supernitride, Sci. Bull. (Beijing). **68**, 1505 (2023).

[26] Y. Gao, Y. Zhang, S. Liu, B. Jin, L. Guo, X. Guo, Z. Yao, P. Wang, and B. Liu, N_{18} ring: A building block for constructing 1D and 2D polymeric nitrogen frameworks, Sci. Bull. (Beijing). **69**, 3860 (2024).

[27] A. Aslandukov *et al.*, Anionic N_{18} macrocycles and a polynitrogen double helix in novel yttrium polynitrides YN_6 and Y_2N_{11} at 100 GPa, Angew. Chem. Int. Ed. **61**, e202207469 (2022).

[28] Y. Zhang, C. Ding, K. Zhang, A. Pakhomova, S. Chen, Y. Ding, S. Jiang, X. Huang, J. Sun, and T. Cui, All-single bonds fused N_{18} macro-rings and N_8 cagelike building blocks stabilized in lanthanum supernitrides, J. Am. Chem. Soc. **146**, 28174 (2024).

[29] A. Aslandukov *et al.*, Stabilization of N_6 and N_8 anionic units and 2D polynitrogen layers in high-pressure scandium polynitrides, Nat. Commun. **15**, 2244 (2024).

[30] M. Bykov, E. Bykova, A. V. Ponomareva, I. A. Abrikosov, S. Chariton, V. B. Prakapenka, M. F. Mahmood, L. Dubrovinsky, and A. F. Goncharov, Stabilization of polynitrogen anions in tantalum–nitrogen compounds at high pressure, Angew. Chem. Int. Ed. **60**, 9003 (2021).

[31] M. Bykov *et al.*, High-pressure synthesis of metal–inorganic frameworks $Hf_4N_{20}{\cdot}N_2$, $WN_8{\cdot}N_2$, and $Os_5N_{28}{\cdot}3N_2$ with polymeric nitrogen linkers, Angew. Chem. Int. Ed. **59**, 10321 (2020).

[32] N. P. Salke, K. Xia, S. Fu, Y. Zhang, E. Greenberg, V. B. Prakapenka, J. Liu, J. Sun, and J. F. Lin, Tungsten hexanitride with single-bonded armchairlike hexazine structure at high pressure, Phys. Rev. Lett. **126**, 065702 (2021).

[33] H. Chen *et al.*, Synthesis and stability of high-energy-density niobium nitrides under high-pressure conditions, Inorg. Chem. **64**, 692 (2025).

[34] M. I. Mc Mahon and R. J. Nelmes, High-pressure structures and phase transformations in elemental metals, Chem. Soc. Rev. **35**, 943 (2006).

[35] J. P. Perdew, A. Ruzsinszky, G. I. Csonka, O. A. Vydrov, G. E. Scuseria, L. A. Constantin, X. Zhou, and K. Burke, Restoring the density-gradient expansion for exchange in solids and surfaces, Phys. Rev. Lett. **100**, 136406 (2008).

[36] G. Kresse and J. Furthmüller, Efficient iterative schemes for *ab initio* total-energy calculations using a plane-wave basis set, Phys. Rev. B **54**, 11169 (1996).

[37] G. Kresse and D. Joubert, From ultrasoft pseudopotentials to the projector augmented-wave method, Phys. Rev. B **59**, 1758 (1999).

[38] A. Togo and I. Tanaka, First principles phonon calculations in materials science, Scr. Mater. **108**, 1 (2015).

[39] A. Carreras, A. Togo, and I. Tanaka, DynaPhoPy: A code for extracting phonon quasiparticles from molecular dynamics simulations, Comput. Phys. Commun. **221**, 221 (2017).

[40] V. L. Deringer, A. L. Tchougréeff, and R. Dronskowski, Crystal orbital Hamilton population (COHP) analysis as projected from plane-wave basis sets, J. Phys. Chem. A **115**, 5461 (2011).

[41] P. C. Müller, C. Ertural, J. Hempelmann, and R. Dronskowski, Crystal orbital bond index: Covalent bond orders in solids, J. Phys. Chem. C **125**, 7959 (2021).

[42] Z. Liu, J. Duan, Z. Qiu, Y. Chen, Z. Yang, Y. Liu, and W. Mi, Decoupled-Hugoniostat: An efficient and universal atomistic dynamics framework for detonation performance prediction (unpublished).

[43] M. Sućeska, Calculation of detonation parameters by EXPLO5 computer program, Mater. Sci. Forum **465**, 325 (2004).

[44] M. Suceska, B. Stimac Tumara, and M. Künzel, Using thermochemical code *EXPLO*5 to predict the performance parameters of explosives, Materia^{a}y Wysokoenergetyczne (High Energy Mater.) (2021).

[45] M. J. Kamlet and S. J. Jacobs, Chemistry of detonations. I. A simple method for calculating detonation properties of C-H-N-O explosives, J. Chem. Phys. **48**, 23 (1968).

[46] See Supplemental Material at http://link.aps.org/supplemental/10.1103/ff7f-yp2m for additional structural parameters, phonon dispersion data and AIMD trajectories, bond angle tables, pressure-dependent bond length evolution, pCOHP bonding curves, RMSD/MSD stability analysis, decomposition enthalpy curves, computational parameter convergence tests, and calculated data validation tables, which includes Refs. [58,59].

[47] J. Zhang, X. Li, X. Dong, H. Dong, A. R. Oganov, and J. M. McMahon, Theoretical study of the crystal structure, stability, and properties of phases in the V-N system, Phys. Rev. B **104**, 134111 (2021).

[48] S. Wang, X. Yu, J. Zhang, L. Wang, K. Leinenweber, D. He, and Y. Zhao, Synthesis, hardness, and electronic properties of stoichiometric VN and CrN, Cryst. Growth Des. **16**, 351 (2016).

[49] S. Asano, K. Niwa, T. Sasaki, N. A. Gaida, and M. Hasegawa, High pressure synthesis and the valence state of vanadium ions for the novel transition metal pernitride, $CuAl_2$-type VN_2, Dalton Trans. **51**, 2656 (2022).

[50] W. Sun *et al.*, A map of the inorganic ternary metal nitrides, Nat. Mater. **18**, 732 (2019).

[51] D. Koch, P. Golub, and S. Manzhos, Stability of charges in titanium compounds and charge transfer to oxygen in titanium dioxide, J. Phys.: Conf. Ser. **1136**, 012017 (2018).

[52] X. Q. Chen, H. Niu, D. Li, and Y. Li, Modeling hardness of polycrystalline materials and bulk metallic glasses, Intermetallics (Barking) **19**, 1275 (2011).

[53] Y. Tian, B. Xu, and Z. Zhao, Microscopic theory of hardness and design of novel superhard crystals, Int. J. Refract. Met. Hard Mater. **33**, 93 (2012).

[54] M. J. Kamlet and C. Dickinson, Chemistry of detonations. III. Evaluation of the simplified calculational method for chapman-Jouguet detonation pressures on the basis of available experimental information, J. Chem. Phys. **48**, 43 (1968).

[55] J. Zhang, A. R. Oganov, X. Li, and H. Niu, Pressure-stabilized hafnium nitrides and their properties, Phys. Rev. B **95**, 020103(R) (2017).

[56] X. Li, Q. Yang, D. Jin, S. Ding, A. Bergara, Y. Yao, L. Zhu, J. Zhao, and G. Yang, Prediction of o-N16: A layered polymeric nitrogen phase, Phys. Rev. B **111**, 134111 (2025).

[57] J. P. Agrawal, *High Energy Materials: Propellants, Explosives and Pyrotechnics* (Wiley-VCH, Weinheim, Germany, 2010).

[58] S. Lin, M. Xu, Y. Liang, X. Yuan, Y. Zhang, F. Wang, J. Hao, and Y. Li, Ambient-pressure recoverable polynitrogen solids assembled by pentazolate rings with high energy density, Inorg. Chem. **61**, 15532 (2022).

[59] M. W. Chase, NIST-JANAF Thermochemical Tables, Fourth Edition, J. Phys. Chem. Ref. Data, 1615 (1998), doi: 10.18434/T42S31.